Journal of Power Sources 247 (2014) 845–851

Contents lists available at ScienceDirect

Journal of Power Sources

journal homepage: www.elsevier.com/locate/jpowsour

Improved electrochemical performance by doping cathode materials $Sr_2Fe_{1.5}Mo_{0.5-x}Ta_xO_{6-\delta}$ ($0.0 \leq x \leq 0.15$) for Solid State Fuel Cell

Junling Meng [a, b], Xiaojuan Liu [a, *], Lin Han [a, b], Yijia Bai [a, b], Chuangang Yao [a, b], Xiaolong Deng [a, b], Xiaodong Niu [a], Xiaojie Wu [a], Jian Meng [a, *]

[a] State Key Laboratory of Rare Earth Resource Utilization, Changchun Institute of Applied Chemistry, Chinese Academy of Sciences, Changchun 130022, PR China
[b] University of Chinese Academy of Sciences, Beijing 100049, PR China

HIGHLIGHTS

- A two-step synthetic method is adopted to obtain SFMTO series compounds.
- The oxygen vacancy concentration increases with the increase of Ta.
- SFMTO TECs match the electrolyte materials better than those of Co-based compounds.
- High performance of SFMTO cathode is demonstrated by low polarization resistance.

ARTICLE INFO

Article history:
Received 4 July 2013
Received in revised form
28 August 2013
Accepted 12 September 2013
Available online 21 September 2013

Keywords:
Solid oxide fuel cells
Cathode materials
Aliovalent substitution
Oxygen vacancy
Conductivity

ABSTRACT

To date great efforts have been devoted to the development of solid oxide fuel cell (SOFC) devices that is able to run at intermediate temperature (IT) and to retain good electrochemical performance as in the high temperature regime. To this end, Tantalum (Ta) is doped into $Sr_2Fe_{1.5}Mo_{0.5-x}Ta_xO_{6-\delta}$ ($0.0 \leq x \leq 0.15$) to further improve the electrochemical performance as the cathode materials for IT-SOFC. Pure orthorhombic $Sr_2Fe_{1.5}Mo_{0.5-x}Ta_xO_{6-\delta}$ ($0.0 \leq x \leq 0.15$) samples, with space group *Pnma* (no. 62), are synthesized by a two-step method and identified via the powder X-ray Rietveld refinements. X-ray photoelectron spectroscopy and thermogravimetry results consistently show that the number of oxygen vacancy increases with the increasing of Ta content. The thermal expansion compatibility of the samples is found to match the electrolyte of $La_{0.9}Sr_{0.4}Ga_{0.1}Mg_{0.2}O_{3-\delta}$ (LSGM) better than that of cobalt-containing electrode compounds. Finally, the higher oxygen vacancy concentration leads to the enhanced ionic conductivity although electrical conductivity is slightly decreased due to the oxygen vacancy blocking. Therefore, Ta-doped $Sr_2Fe_{1.5}Mo_{0.5}O_{6-\delta}$ is proved to be a promising candidate for future cathode materials of IT-SOFC.

1. Introduction

Solid oxide fuel cells (SOFCs) are electrochemical energy conversion devices that possess high energy conversion efficiency with fuel flexibility [1]. A SOFC is composed of three main components, the anode (for fuel oxidation), the cathode (for oxygen reduction), and the electrolyte, plus an interconnect materials. The electrolyte is a dense layer of ceramic that conducts oxygen ions. Its electronic conductivity must be kept as low as possible to prevent losses from leakage currents. The most widely used electrolyte materials are yttria-stabilized zirconia (YSZ) and samarium-doped ceria [2–4]. Electrode materials must be very porous to allow easy diffusion of the fuel and ideally must conduct both oxygen anions and electrons. Usually, the electrode materials used in SOFC become electrically and ionically active only at high temperatures, typically between 700 and 1000 °C. Unfortunately, the high thermal stress could cause the delamination at cathode/electrolyte interface or cracking electrolyte during operating temperature range, resulting in premature aging of interconnect materials [5–7]. Thus an active research is focusing on the development of intermediate temperature (IT) SOFCs, meaning that they operate within the range of 500–800 °C so as to diminish premature aging of the SOFC materials, thereby improving the durability, stability and reliability of the devices [8,9]. Therefore, great efforts have been devoted to

* Corresponding authors. Tel.: +86 431 85262030; fax: +86 431 85698041.
E-mail addresses: lxjuan@ciac.jl.cn (X. Liu), jmeng@ciac.jl.cn (J. Meng).

0378-7753/$ – see front matter © 2013 Elsevier B.V. All rights reserved.
http://dx.doi.org/10.1016/j.jpowsour.2013.09.049

finding electrode materials that show the following properties: (1) good electronic conductivity; (2) good ionic diffusivity; (3) good catalytic activity for the oxygen reduction reaction (ORR); and (4) a thermal expansion coefficient compatible with the electrolyte. The ideal material then must be a mixed ionic electronic conductor (MIEC) [10].

Among many proposed systems, electrodes based on $Sr_2Fe_{1.5}Mo_{0.5}O_{6-\delta}$ (SFMO) have been found to be remarkably efficient for IT-SOFCs [11–13]. In particular, SFMO has been used as both the cathode and anode material in symmetrical configuration, demonstrating not only chemical compatibility with the electrolyte but also chemical stability in both reducing and oxidizing conditions, and remarkable electrocatalytic performance for both oxygen reduction and fuel oxidation [14]. After all, SFMO exhibit the characteristic behavior of a mixed ionic and electronic conductor with good ionic and electrical conductivity. However, detailed comparison with other prototypical cathode compounds, such as $(Ba_{0.5}Sr_{0.5})_{1-x}Co_{0.8}Fe_{0.2}O_{3-\delta}$ ($x > 0$) [9], indicates that its ionic conductivity is still required to be improved although its electrical conductivity is high enough to fulfill the practical application.

The electrochemical performance can further be improved by aliovalent substitution and this strategy has been widely used to improve the oxygen ionic conductivity. For example, to develop CeO_2-based oxides with improved ionic conductivity, aliovalent doping of many cations, such as Gd, Sm, Ca and La have been investigated extensively, and the highest level of ionic conductivity was reported in Gd- and Sm-doped $Ce_{1-x}M_xO_{2-\delta}$ compositions [15–18]. In this work, we try to replace Mo^{6+} with Ta^{5+} to improve the ionic conductivity by the increase of oxygen vacancy concentrations. This study presents the effect of Ta doping on SFMO properties including lattice structure, element valence, electronic conductivity, interfacial polarization resistance, chemical compatibility and thermal expansion behavior. It is found that Ta-doped SFMO present a remarkably high electrochemical performance for future technological applications.

2. Experimental

2.1. Sample preparation

$Sr_2Fe_{1.5}Mo_{0.5-x}Ta_xO_{6-\delta}$ (SFMTO, $0.0 \le x \le 0.15$) was synthesized via a two-step method, namely combined modified Pechini method [19] with solid–state reactions. The first step is to prepare the precursor powder by sol–gel technique with citric acid and polyethylene glycol as the chelating agent and $Sr(NO_3)_2$ (99.97%), $FeC_2O_4{\cdot}2H_2O$ (99%), $(NH_4)_6Mo_7O_{24}{\cdot}4H_2O$ (99.9%) as the starting materials. Stoichiometric quantities of the raw materials were dissolved in deionized water under heating and stirring. An appropriate amount of citric acid was added into the solution, and polyethylene glycol was then dissolved in the above clear yellowish precursor. Subsequently, the solution was transferred to the pottery evaporating wares and vaporized in the water bath at 85 °C overnight. Black precursor was obtained followed by heating the dry gel onto the gas burner for 5 min. The next step was solid–state reaction. Mixed the above precursor powders with Ta_2O_5 (99.9%) in stoichiometric ratio, and first burnt at 900 °C in air for 10 h to eliminate the organic matter. The calcined powders were pelletized and finally annealed at 1400 °C in air for 10 h to form pure phase. $La_{0.9}Sr_{0.4}Ga_{0.1}Mg_{0.2}O_{3-\delta}$ (LSGM) and $Ce_{0.8}Sm_{0.2}O_{2-\delta}$ (SDC) electrolyte powders were prepared by sol–gel method as described elsewhere [20,21].

Symmetrical cells with SFMTO|LSGM|SFMTO configuration were fabricated by screen-printing technique. Dense LSGM pellets (18 mm in diameter) were prepared by pressing the powders under 40 MPa, and then followed by isostatic cool pressing under 270 MPa, finally sintered at 1400 °C for 10 h. SFMTO cathode slurries were made by mixing the powders with binder (α-terpineol and ethylene cellulose) and coated on both surfaces of LSGM with 500 μm thickness by screen-printing, and then fired at 1400 °C in air for 2 h at ramping rate of 2 °C min^{-1}. The resulting electrode had a thickness of ~15 μm and an effective area of 0.25 cm^2. Silver paste was attached to both sides as a current collector, which was heated to 600 °C for 30 min in air.

2.2. Characterizations

The initial crystal structure of the samples were characterized by powder X-ray diffraction (XRD) in a Bruker AXS D8 Advance diffractometry (40 kV, 40 mA) with Cu-Ka radiation ($\lambda = 1.5418$ Å), and employed a scan rate of 8 deg min^{-1} in the 2θ range of 15°–85°. Rietveld refinement data of the sample was collected on Rigaku D/max-2500 diffractometry (40 kV, 200 mA) with Cu-Ka radiation ($\lambda = 1.5418$ Å), and adopted a step scan rate of 0.02° in the 2θ range of 10°–120°. The structure parameters of the SFMTO were acquired using the GSAS-EXPGUI software [22]. Hitachi S-4800 high resolution FE-SEM equipped with the energy dispersive X-ray spectrometer (EDS) analyzer (XP30, Philips) was used to observe the micrographs and the chemical composition of the sintered pellets. X-ray photoelectron spectroscopy (XPS) data were collected on a VG ESCALAB 250 Electron Spectrometer with a monochromatic Al Kα (1486.6 eV) at 12 kV and 20 mA, and all binding energies were referred to the C 1s peak (284.6 eV). Differential Scanning Calorimetry/Thermogravimetry (DSC/TG) were carried out on a NETZSCH STA 449F3 from room temperature to 1100 °C with a heating rate of 10 °C min^{-1} under nitrogen atmosphere. The sample and reference were situated in platium crucibles, and α-Al_2O_3 was the inert reference.

Measurement of the thermal expansion coefficient and electrical conductivity required the densified sintered pellets through isostatic cool pressing under 270 Mpa, and fired at 1400 °C for 10 h. The relative density of sintered pellets could achieve ~95%, which were determined by Archimedes method. The thermal expansion study of the dense ceramic samples, which was measured on rectangular bars (~5 mm × 5 mm × 25 mm), was performed on a NETZSCH DIL 402C apparatus from room temperature to 900 °C in flowing air. The electrical conductivity was measured using Keithley 2400 SourceMeter (Keithley Instruments, Inc.) by Van der Pauw four-probe dc method in temperature range from 850 °C to 200 °C with an interval of 50 °C in air. Silver wire and silver paste were used to make the four probes. The measured conductivity can be corrected with the equation below [23]:

$$\sigma_{corr} = \frac{\sigma_{app}}{2(d_{rel}/100 - 0.5)} \quad (1)$$

where σ_{corr}, d_{rel} and σ_{app} are the porosity-corrected conductivity, the relative density and the measured apparent conductivity, respectively. Impedance measurements were performed on symmetrical cells of SFMTO|LSGM|SFMTO from 850 °C to 650 °C in steps of 50 °C. The polarization resistances of the symmetrical cells were recorded on Autolab Electrochemical Instruments-PGSTAT302 under an open circuit voltage conditions (OCV) in the frequency range from 100 KHz to 0.01 Hz with an amplitude signal of 10 mV, which was controlled by the FRA 4.9.006 software.

3. Results and discussion

3.1. Structural characterization

The XRD patterns of $Sr_2Fe_{1.5}Mo_{0.5-x}Ta_xO_{6-\delta}$ ($0.0 \le x \le 0.15$) series are shown in Fig. 1. No impurity phases were observed after

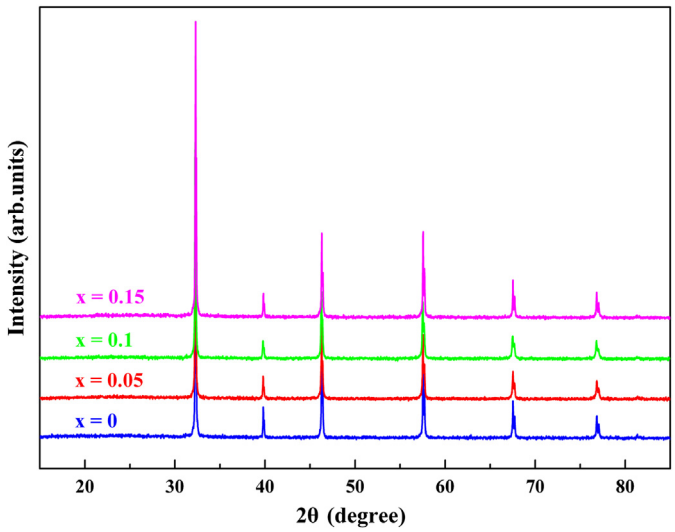

Fig. 1. Powder X-ray diffraction patterns of the $Sr_2Fe_{1.5}Mo_{0.5-x}Ta_xO_{6-\delta}$ ($0.0 \le x \le 0.15$) series at room temperature.

fired at 1400 °C for 10 h. The crystal structure is an important parameter that influence ionic and electronic transport and mechanical properties. The structure of SFMO has been reported as cubic ($Fm\bar{3}m$) or orthorhombic (*Pnma*) space group from different synthesis conditions according to the previous reports [24,25]. The above two space groups were chosen as the models for Rietveld refinement, and better fits and smaller χ^2_{red} value (1.759) were obtained when *Pnma* (no. 62) model was applied. The obtained atomic and structural parameters by Rietveld refinement are listed in Table 1 and Table 2, and the goodness of fit is illustrated in Fig. 2 taking the sample of $x = 0.1$ as an example. The structural difference of perovskite oxides stem from the ordering of B-site cations and titling of BO_6 octahedra, which makes the structure very flexible and complicated [26]. The B-sites are shared by Fe, Mo and Ta, and the possibility of the oxygen vacancies created by aliovalent substitution will further provide the driving force for disordering of B-sites ions. In this regard, this kind of structural change can be attributed to the tilting of the BO_6 (B = Fe, Mo or Ta) octahedra.

3.2. Microstructure and elemental compositions

The SEM micrographs of the as-prepared densified pellet of $Sr_2Fe_{1.5}Mo_{0.4}Ta_{0.1}O_{6-\delta}$ and the cross section of SFMTO|LSGM|SFMTO are shown in Fig. 3. From the Fig. 3a, the particles show homogeneous distribution, and the average size is about 5 μm. There are some small pores among the grains. The pores are barriers to the electrical conduction, therefore, the measurement of electrical conductivity required densified pellets. The relative density of the pellet obtained by Archimedes method is about 95%. Fig. 3b shows the typical SEM micrographs of the cross section of symmetrical fuel cell of SFMTO|LSGM|SFMTO. The boundary between electrode and electrolyte is clear, and the cathode layer adheres to the electrolyte fairly well, which would induce a decrease in the polarization resistance of the cathode. Hence, a high electrochemical performance can be expected. The elemental compositions and homogeneity of $Sr_2Fe_{1.5}Mo_{0.5-x}Ta_xO_{6-\delta}$ series are analyzed by EDS through mapping mode, five parallel tests were performed for 15 min to each sample. The average atomic concentration of the experimental value as compared to the nominal stoichiometry is presented in Table 3. The experimental values are in good agreement with the nominal stoichiometry.

Table 1
Atomic parameters for $Sr_2Fe_{1.5}Mo_{0.4}Ta_{0.1}O_{6-\delta}$ from Rietveld refinement of powder X-ray diffraction data.

	Site	*x*	*y*	*z*	Uiso (Å^2)	Occupancy
Sr	4c	0.4983(7)	0.25	0.9996(9)	0.0142(9)	1.0
Fe	4a	0	0	0	0.0114(4)	0.75
Mo	4a	0	0	0	0.0114(4)	0.20
Ta	4a	0	0	0	0.0114(4)	0.05
O (1)	4c	0.5157(7)	0.25	0.5080(1)	0.02	1.0
O (2)	8d	0.2347(8)	0.0077(9)	0.2540(1)	0.0211(1)	1.0

Table 2
Structural refinement result for $Sr_2Fe_{1.5}Mo_{0.4}Ta_{0.1}O_{6-\delta}$ from Rietveld refinement of powder X-ray diffraction data.

Temperature (K)	298
a (Å)	5.5475(1)
b (Å)	7.8341(2)
c (Å)	5.5416(2)
Volume (Å^3)	240.83(1)
R_p (%)	7.79
R_{wp} (%)	10.47
χ^2	1.759
Fe/Mo/Ta–O (2) × 2 (Å)	1.91871(4)
Fe/Mo/Ta–O (1) × 2 (Å)	1.96098(6)
Fe/Mo/Ta–O (2) × 2 (Å)	2.00667(4)

3.3. X-ray photoelectron spectroscopy

The mixed-valent Fe^{2+}/Fe^{3+} and Mo^{5+}/Mo^{6+} coupling on B sites plays an important role on the electrochemical characteristics of $Sr_2Fe_{1.5}Mo_{0.5-x}Ta_xO_{6-\delta}$ series. To verify the chemical state of Fe and Mo on B-site, we have analyzed the XPS spectra with the fitting program XPS PEAK 4.1 at room temperature. The Fe 2p and Mo 3d core level spectra are shown in Fig. 4. Each of them can be resolved into two components, namely Fe^{2+}, Fe^{3+} and Mo^{5+}, Mo^{6+}. The percentage contributions of the valence states, average valence states of Fe and Mo and the approximate value of δ are given in Table 4. As can be seen in Table 4, the average valence states of Fe and Mo decreased gradually. According to the average valence

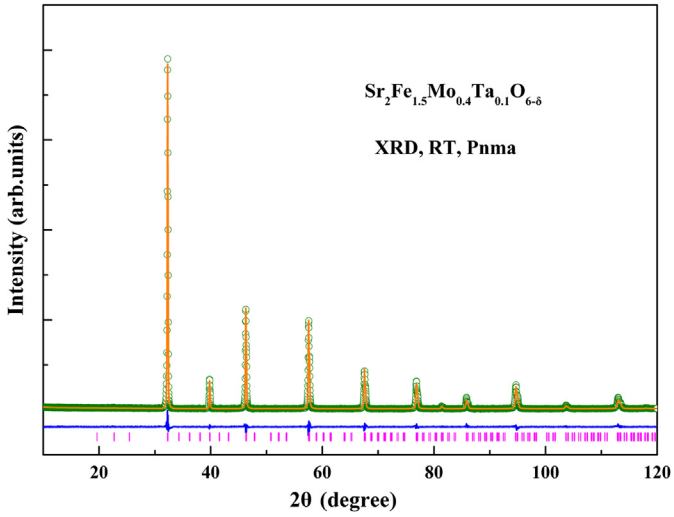

Fig. 2. Rietveld refinement of powder X-ray diffraction data for $Sr_2Fe_{1.5}Mo_{0.4}Ta_{0.1}O_{6-\delta}$. Observed (green circle), calculated (origen solid line), difference (blue line), and the allowed Bragg reflections (pink vertical markers) profiles are shown. (For interpretation of the references to color in this figure legend, the reader is referred to the web version of this article.)

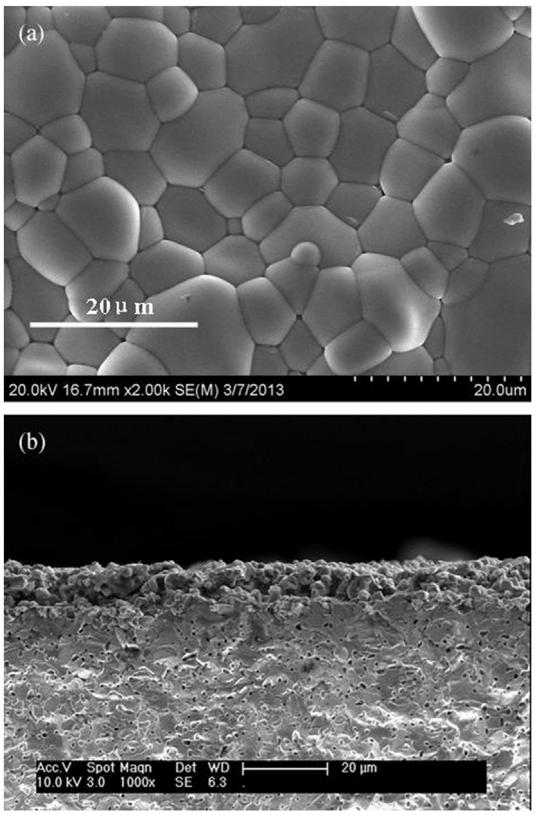

Fig. 3. SEM images (a) $Sr_2Fe_{1.5}Mo_{0.4}Ta_{0.1}O_{6-\delta}$, (b) cross section SEM image of symmetrical fuel cell of SFMTO|LSGM|SFMTO.

states of Fe and Mo, we can get the approximate value of δ. The δ increases with doping content. Therefore, our XPS results confirmed that the number of oxygen vacancies increase with the Ta doping. Consequently, the oxide ion conductivity should increase due to an increase of oxygen vacancy concentrations. Aliovalent substitution can introduce charge imbalance into crystals, thus, some oxygen vacancies will form in order to achieve the balance, namely, the formation of point defects in crystals after replacement, resulting in the improvement of the oxide ionic conductivity. This behavior is further supported by the result of impedance analysis in the follow.

3.4. Thermogravimetric analysis

Fig. 5a present the TG and DSC curves for $Sr_2Fe_{1.5}Mo_{0.4}Ta_{0.1}O_{6-\delta}$ carried out in nitrogen between room temperature and 1100 °C. There is a subtle weight loss (~0.2%) from room temperature to 400 °C, which is ascribed to the dehydration and surface oxygen desorption. The TG curve began to show a sudden decrease in stoichiometry at about 500 °C, which involves the B-site ions reduction, corresponding to the loss of lattice oxygen. An endothermic peak is observed on the DSC curve at about 900 °C, which may be related to a subtle order-disorder transformation concerning the rearrangement of oxygen vacancies per formula unit accompanied by very small heat transfer [27]. The unaltered XRD patterns confirm the absence of phase transition or decomposition after the thermal treatment in nitrogen. Thermogravimetric curves for $Sr_2Fe_{1.5}Mo_{0.5-x}Ta_xO_{6-\delta}$ series are shown in Fig. 5b. The weight loss increase with increasing Ta substitution, and the oxygen content decreased continuously. This behavior is further supported by the result of thermal expansion analysis.

Table 3
The comparison between nominal and experimental stoichiometry of $Sr_2Fe_{1.5}Mo_{0.5-x}Ta_xO_{6-\delta}$ ($0.0 \le x \le 0.15$).

Sample	Element			
	Sr	Fe	Mo	Ta
$Sr_2Fe_{1.5}Mo_{0.45}Ta_{0.05}O_{6-\delta}$				
Nominal value	2	1.5	0.45	0.05
Experimental value	2.062	1.432	0.4333	0.07310
$Sr_2Fe_{1.5}Mo_{0.4}Ta_{0.1}O_{6-\delta}$				
Nominal value	2	1.5	0.4	0.1
Experimental value	2.051	1.452	0.3893	0.1076
$Sr_2Fe_{1.5}Mo_{0.35}Ta_{0.15}O_{6-\delta}$				
Nominal value	2	1.5	0.35	0.15
Experimental value	2.042	1.485	0.3411	0.1549

3.5. Thermal expansion behavior

TECs of both the electrolyte and electrode layers must be well matched to ensure long-term SOFC operational stability. Thus the acceptable dimensional change of TECs for an IT cathode is less than $30 \times 10^{-6}\ K^{-1}$ under the condition of taking SDC or LSGM as the electrolyte material. Thermal expansion behavior of the samples between room temperature (RT) to 900 °C in air is displayed in Fig. 6. The average TECs of $Sr_2Fe_{1.5}Mo_{0.45}Ta_{0.05}O_{6-\delta}$ and $Sr_2Fe_{1.5}Mo_{0.4}Ta_{0.1}O_{6-\delta}$ are about $15.0 \times 10^{-6}\ K^{-1}$ and $16.9 \times 10^{-6}\ K^{-1}$ in air, respectively, a little higher than that of SFMO [11] but much lower than that of the Co-base cathodes [28]. The TECs of $Sr_2Fe_{1.5}Mo_{0.5-x}Ta_xO_{6-\delta}$ and LSGM electrolyte ($11.1 \times 10^{-6}\ K^{-1}$) are much closer than that of Co-base cathodes. The result also show that the TECs increases with increasing Ta content. Because the ionic radius of Ta^{5+} ($r = 0.78$ Å) is larger than that of Mo^{6+} ($r = 0.59$ Å) and Mo^{5+} ($r = 0.61$ Å), thus the a little lattice expansion contributes to the increase in TECs with Ta doping. TECs can also increase with increasing oxide ion vacancies because of a reduction in the electrostatic attractive force between the cations and anions, and a reduction of smaller Fe^{3+} or Mo^{6+} to larger Fe^{2+} or Mo^{5+} ions at high temperature [29]. The temperature at which the expansion curve deviates from linearity showing a complex changing trend with increasing Ta content, which may attribute to the influence of the formation of oxide ion vacancies on the lattice expansion. This conclusion is excellent agreement with that determined by TG analysis. The same can therefore be inferred for the sample of $Sr_2Fe_{1.5}Mo_{0.35}Ta_{0.15}O_{6-\delta}$.

3.6. Electrical conductivity analysis

Electrical conductivity of samples was measured by the Van der Pauw four–probe dc method. An almost parabola relationship between ln (σ T) and $1000/T^{-1}$ is shown in Fig. 7. The insert picture is the conductivity of samples versus temperature in air. It can be observed that the electrical conductivity exhibits Arrhenius–like temperature dependence, and the dc-conductivity of $Sr_2Fe_{1.5}Mo_{0.5-x}Ta_xO_{6-\delta}$ ($0.0 \le x \le 0.15$) series decreased gradually with increasing Ta content. The conductivity behavior of all samples exhibits a monotonic increase from room temperature to around 500 °C, which is consistent with the small polaron hopping mechanism [30]. It has been well known that small polaron hopping is a thermally activated process at lower temperature (<500–600 °C) and that the conductivity of small polaron increases with increasing temperature. However, the conductivity decreased above a transition temperature of about 500 °C, which can be attributed to the formation of oxygen vacancies at high temperature (>550 °C). At this moment, the small polaron hopping is not the major transport mechanism but rather the oxygen vacancy compensation mechanism above this transition temperature [31].

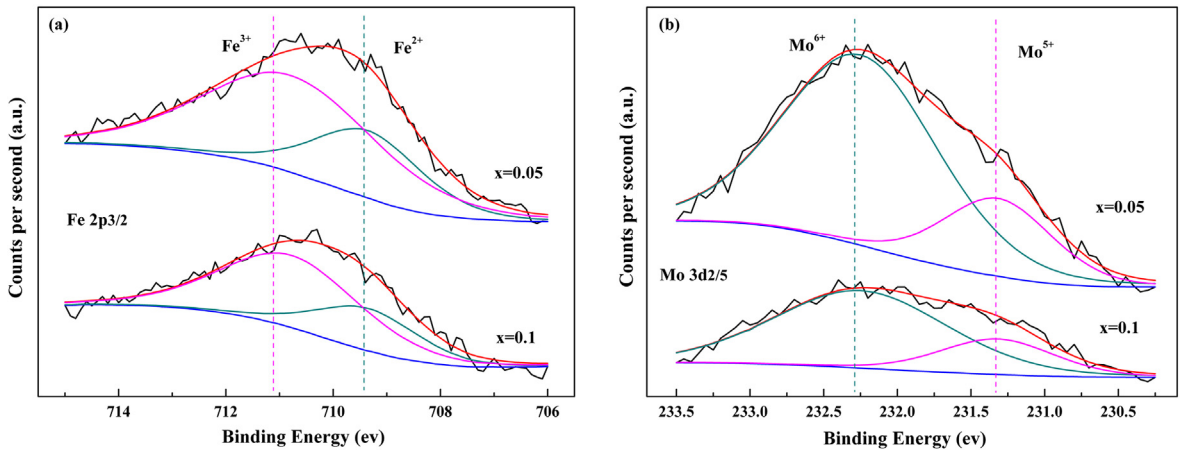

Fig. 4. XPS spectra and curve-fitting of (a) Fe 2p and (b) Mo 3d core-level of different Ta content at room temperature.

The formation of oxygen vacancies accompanied by a reduction of Fe^{3+} to Fe^{2+} or Mo^{6+} to Mo^{5+} at higher temperature causes a decrease in the charge carrier concentration, resulting in a decrease in conductivity. In our case, the dc-conductivity reduced by about an order of magnitude power compared with previous report [14]. The main reason for this conductive behavior is that the substantial oxygen vacancies produced by partial substitution on Mo-site by Ta^{5+} ion could affect the percolation path (Fe–O–Fe) for electrons or holes hopping at higher temperature, then some electrons or holes are blocked by oxygen vacancies, leading to lower electrical conductivity [26]. Besides, it is well known that the variable cation oxidation states introduce electronic conductivity, the Ta^{5+} substitution would also lead to a decrease in electronic conductivity because of its fixed valence state. However, although the electrical conductivity is decreased due to the doping and/or synthetic method, their absolute values are still higher than those of $(Ba_{0.5}Sr_{0.5})_{1-x}Co_{0.8}Fe_{0.2}O_{3-\delta}$ ($x > 0$) in Ref. [9] with their vales to be 43.45, 35.89, 29.84 and 22.74 S cm^{-1} for the samples of $x = 0.0$, 0.05, 0.10 and 0.15, respectively, which is still high enough to fulfill the practical applications.

3.7. Chemical compatibility

A further important issue for the application of the current materials is the stability. The chemical compatibility of the cathode with electrolyte (SDC, LSGM) materials is shown in Fig. 8. A mixture of $Sr_2Fe_{1.5}Mo_{0.4}Ta_{0.1}O_{6-\delta}$ and (SDC, LSGM) in weight ratio of 1:1 were milled and calcined at 1000 °C for 12 h in air. SDC (Fig. 8a) is in the fluorite structure while LSGM (Fig. 8b) is in perovskite-type structure. XRD results demonstrate that no new identifiable peak or obvious diffraction peak shift could be observed, thus indicating the absence of observable reaction and confirming excellent chemical compatibility between our investigated electrode and these two prototypical electrolyte materials.

Table 4
The proportion of Fe and Mo valence states, average valence states of Fe and Mo and the approximate value of δ in $Sr_2Fe_{1.5}Mo_{0.5-x}Ta_xO_{6-\delta}$ ($0.05 \le x \le 0.15$).

Doping content	Fe $2p_{3/2}$		Mo $3d_{5/2}$		Average valence		δ
	Fe^{3+} (%)	Fe^{2+} (%)	Mo^{5+} (%)	Mo^{6+} (%)	Fe	Mo	
$x = 0.05$	69.73	30.27	22.36	77.64	2.697	5.776	0.55
$x = 0.1$	69.64	30.36	23.32	76.68	2.696	5.767	0.57
$x = 0.15$	66.74	32.26	32.33	67.67	2.667	5.677	0.63

3.8. Impedance analysis

The cathode performance of the studied compounds was evaluated by impedance spectroscopy in air performing on a symmetrical cell configuration. Fig. 9 shows the impedance spectra of

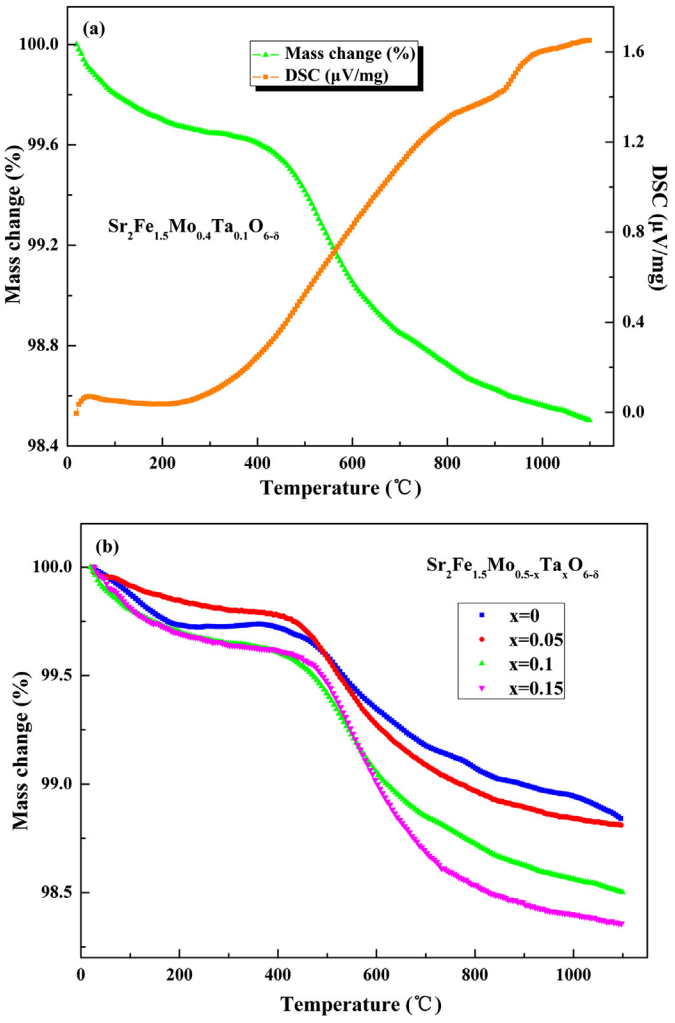

Fig. 5. (a) Thermal analysis curves of $Sr_2Fe_{1.5}Mo_{0.4}Ta_{0.1}O_{6-\delta}$ recorded in nitrogen. (b) Thermogravimetric analysis of $Sr_2Fe_{1.5}Mo_{0.5-x}Ta_xO_{6-\delta}$ ($0.0 \le x \le 0.15$).

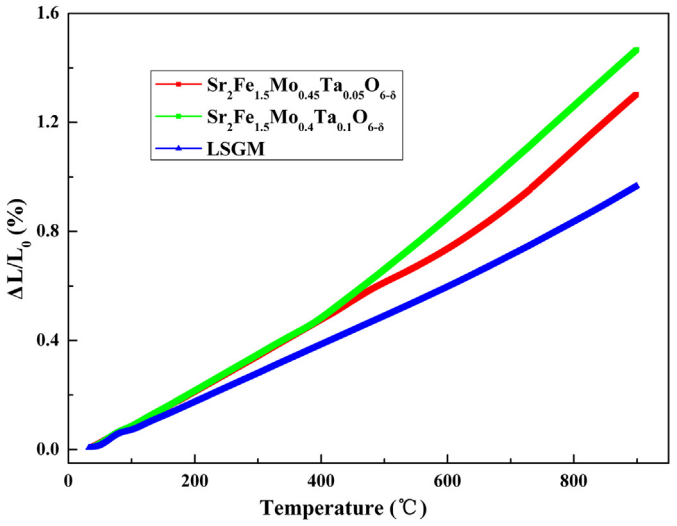

Fig. 6. Thermal expansion profiles of electrode (SFMTO) and electrolyte (LSGM) materials.

SFMTO|LSGM|SFMTO in different doping content and different temperature range under open–circuit conditions. The Nyquist plots of the symmetrical cell can approximately be considered as a section of arc, no addition arc was observed at the low–frequency range, which suggests the absence of gaseous diffusion polarization resistance. The difference of intercepts with the real axis between high frequency and low frequency corresponds to the polarization resistance of the cathode/electrolyte interface. The profiles clearly present that the polarization resistance is decreased gradually with the increasing temperature and doping content. The polarization resistances of $Sr_2Fe_{1.5}Mo_{0.5-x}Ta_xO_{6-\delta}$ ($0.0 \le x \le 0.15$) are about 0.22, 0.20, 0.16 and 0.087 Ω cm^2 at 800 °C, respectively, which is much lower than those reported in previous paper [14], and similarly to those in Ref. [11] after doped with Ta. Another point worthy of mentioned is that this value is slightly higher than that of Co-based cathode $(Ba_{0.5}Sr_{0.5})_{1-x}Co_{0.8}Fe_{0.2}O_{3-\delta}$ ($x > 0$) [9] under similar conditions. Generally, oxygen reduction reaction is strongly dependent on oxygen surface adsorption and oxide ionic diffusivity. The oxygen reduction reaction on cathode can be expressed as:

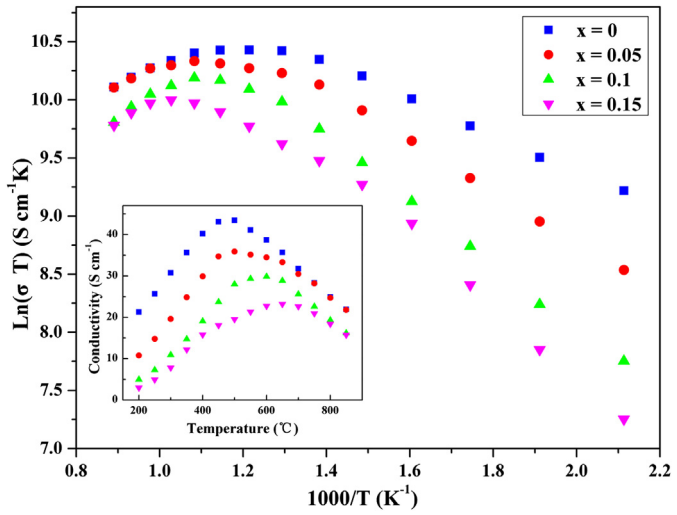

Fig. 7. Temperature dependence of dc-conductivity of $Sr_2Fe_{1.5}Mo_{0.5-x}Ta_xO_{6-\delta}$ ($0.0 \le x \le 0.15$) in air.

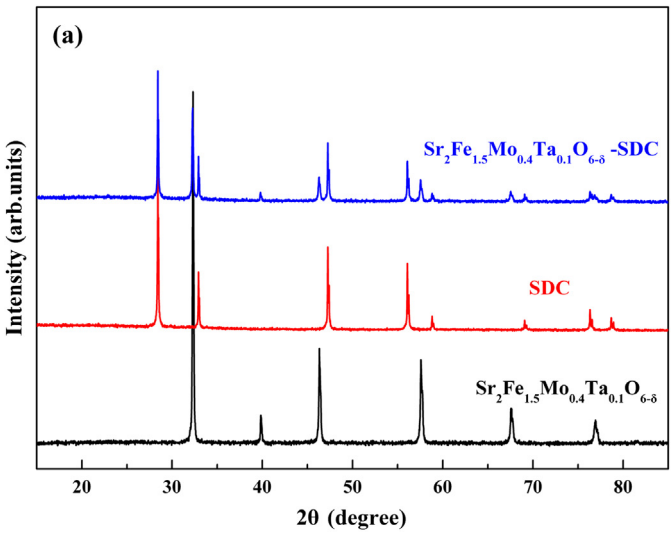

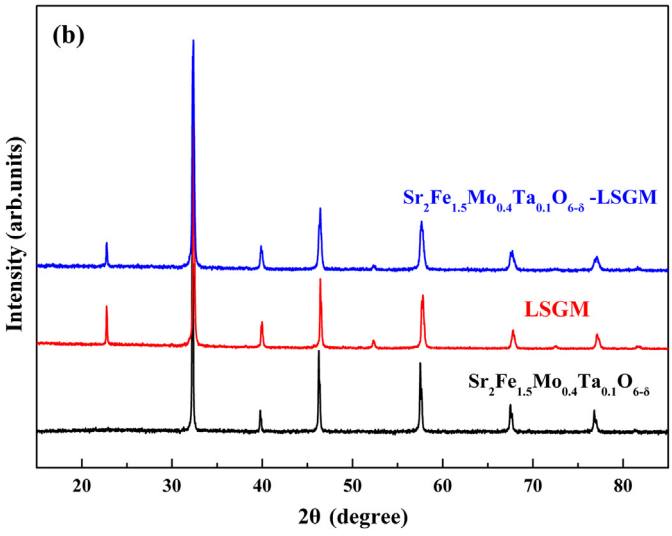

Fig. 8. XRD profiles of a mixture of $Sr_2Fe_{1.5}Mo_{0.4}Ta_{0.1}O_{6-\delta}$ and different electrolyte materials (a) SDC, (b) LSGM after fired at 1000 °C for 12 h. The XRD patterns of pure $Sr_2Fe_{1.5}Mo_{0.4}Ta_{0.1}O_{6-\delta}$ and electrolytes are also presented for comparison.

$$O_2 + 2V_O^{\bullet\bullet} + 4e^- \rightarrow 2O^{2-} \quad (3)$$

The oxygen vacancy ($V_O^{\bullet\bullet}$) can be seen as the ionic charge carriers, namely, oxygen vacancies is apt to the adsorption and diffusion of oxygen ions. Therefore, the oxygen ion conductivity increases with the increasing $V_O^{\bullet\bullet}$. It indeed illustrate that aliovalent substitution on Mo-site by Ta ion improve the cathode performance. This consequence is in excellent agreement with that determined by XPS analysis.

4. Conclusions

Synthesis, characterization, and electrochemical properties of $Sr_2Fe_{1.5}Mo_{0.5-x}Ta_xO_{6-\delta}$ ($0.0 \le x \le 0.15$) perovskite as cathode materials for IT-SOFCs have been presented and discussed in this paper. With the aim to decrease the polarization resistance and improve the electrochemical performance, we adopted aliovalent substitution to introduce oxygen vacancy, which is closely related to the adsorption and diffusion of oxygen on the electrode surface. XRD, XPS, SEM-EDS, TG-DSC and TEC analysis has been undertaken to reach a precise determination of its defect chemistry. The results

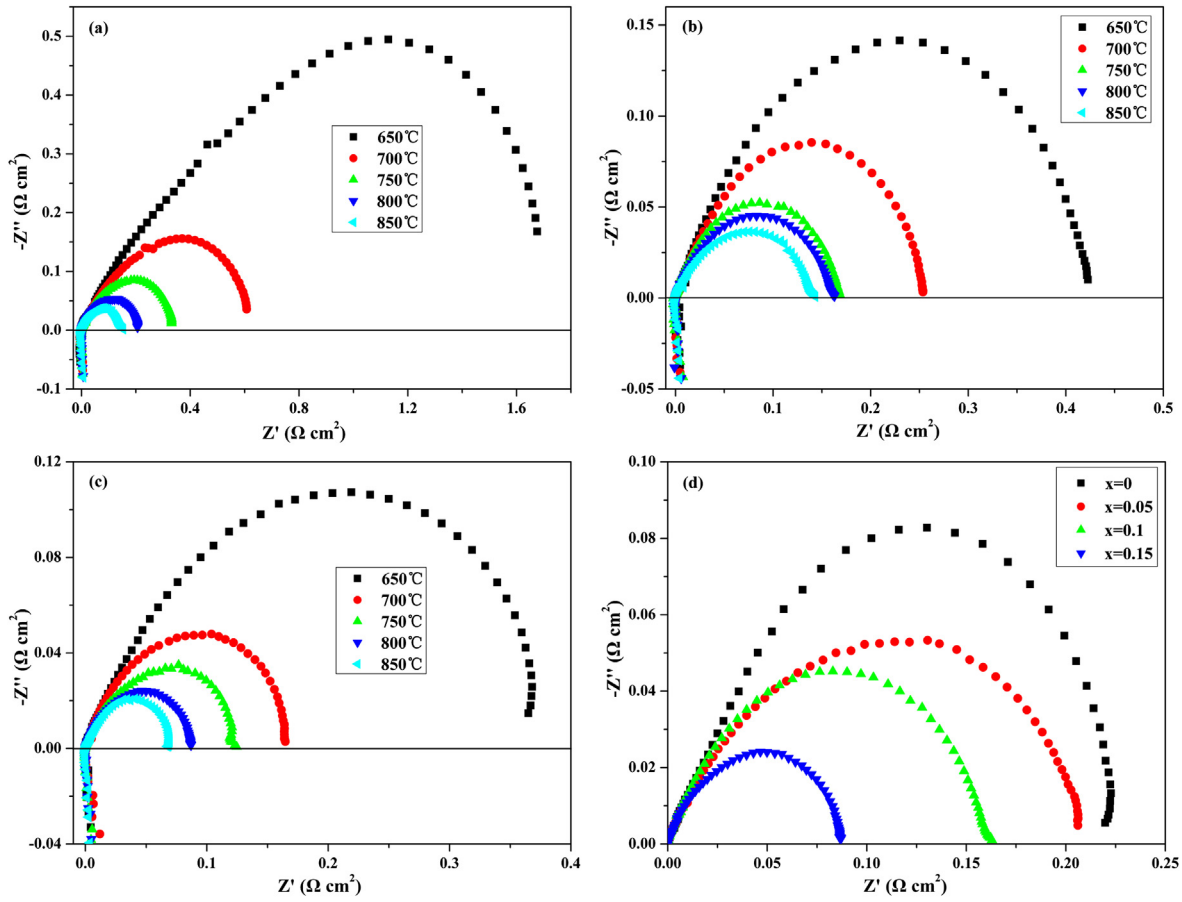

Fig. 9. Impedance spectra of $Sr_2Fe_{1.5}Mo_{0.5-x}Ta_xO_{6-\delta}$ ($0.0 \le x \le 0.15$) cathode measured with a symmetrical cell SFMTO|LSGM|SFMTO configuration in the temperature range of 650–850 °C in air. (a) $x = 0.05$, (b) $x = 0.1$, (c) $x = 0.15$, (d) The comparison of impedance spectra among different doping content at 800 °C.

show that the oxygen vacancies increased with the Ta doping, which makes it easy for improvement in oxygen ion conductivity. The polarization resistance is much lower than the previous reports at the same temperature. Besides, their thermal expansion is found to remarkably match the widely-used electrolyte materials and chemical stability is also investigated. Therefore, $Sr_2Fe_{1.5}Mo_{0.5-x}Ta_xO_{6-\delta}$ ($0.0 \le x \le 0.15$) can be a good candidate for IT-SOFCs cathode materials.

Acknowledgments

This work was supported by the National Natural Science Foundation of China under grants no. 20871023, 51002148, 21071141, and 20921002.

References

[1] R.M. Ormerod, Chem. Soc. Rev. 32 (2003) 17–28.
[2] S.Q. Hui, J. Roller, S. Yick, X.G. Zhang, C. Decès–Petit, Y.S. Xie, R. Maric, D. Ghosh, J. Power Sources 172 (2007) 493–502.
[3] B.C.H. Steele, A. Heinzel, Nature 414 (2001) 345–352.
[4] L. Rose, M. Menon, K. Kammer, O. Kesler, P.H. Larsen, Adv. Mater. Res. 15 (2007) 293–298.
[5] L. Yang, S.Z. Wang, K. Blinn, M.F. Liu, Z. Liu, Z. Cheng, M.L. Liu, Science 326 (2009) 126–129.
[6] A. Orera, P.R. Slater, Chem. Mater. 22 (2010) 675–690.
[7] A. Aguadero, C. Calle, J.A. Alonso, M.J. Escudero, M.T. Fernández–Díaz, L. Daza, Chem. Mater. 19 (2007) 6437–6444.
[8] Q.J. Zhou, T.M. He, Y. Ji, J. Power Sources 185 (2008) 754–758.
[9] W. Zhou, R. Ran, Z.P. Shao, W.Q. Jin, N.P. Xu, J. Power Sources 182 (2008) 24–31.
[10] Y. Li, Y.N. Kim, J.G. Cheng, J.A. Alonso, Z.W. Hu, Y.Y. Chin, T. Takami, M.T. Fernández, Díaz, H.J. Lin, C.T. Chen, L.H. Tjeng, A. Manthiram, J.B. Goodenough, Chem. Mater. 23 (2011) 5037–5044.
[11] G.L. Xiao, Q. Liu, F. Zhao, L. Zhang, C.R. Xia, F.L. Chen, J. Electrochem. Soc. 158 (2011) B455–B460.
[12] Q. Liu, D.E. Bugaris, G.L. Xiao, M. Chmara, S.G. Ma, H.C. Loye, M.D. Amiridis, F.L. Chen, J. Power Sources 196 (2011) 9148–9153.
[13] G.L. Xiao, C. Jin, Q. Liu, A. Heyden, F.L. Chen, J. Power Sources 201 (2012) 43–48.
[14] Q. Liu, X.H. Dong, G.L. Xiao, F. Zhao, F.L. Chen, Adv. Mater. 22 (2010) 5478–5482.
[15] S.D. Park, J.M. Vohs, R.J. Gorte, Nature 404 (2000) 265–267.
[16] B.C.H. Steele, Solid State Ionics 129 (2000) 95–110.
[17] M. Mogensen, N.M. Sammes, G.A. Tompsett, Solid State Ionics 129 (2000) 63–94.
[18] H. Iwahara, T. Esaka, T. Mangahara, J. Appl. Electrochem 18 (1988) 173–177.
[19] J.C. Pérez–Flores, D. Pérez–Coll, S. García–Martín, C. Ritter, G.C. Mather, J. Canales–Vázquez, M. Gálvez–Sánchez, F. García–Alvarado, U. Amador, Chem. Mater. 25 (2013) 2484–2494.
[20] K.Q. Huang, M. Feng, J.B. Goodenough, J. Am. Ceram. Soc. 79 (1996) 1100–1104.
[21] W. Huang, P. Shuk, M. Greenblatt, Solid State Ionics 100 (1997) 23–27.
[22] B.H. Toby, J. Appl. Crystallogr. 34 (2001) 210–213.
[23] X.B. Chen, S.P. Jiang, J. Mater. Chem. A 1 (2013) 4871–4878.
[24] G.Y. Liu, G.H. Rao, X.M. Feng, H.F. Yang, Z.W. Ouyang, W.F. Liu, J.K. Liang, J. Alloys Compd. 353 (2003) 42–47.
[25] A.B. Muñoz –García, D.E. Bugaris, M. Pavone, J.P. Hodges, A. Huq, F.L. Chen, H.C. Loye, E.A. Carter, J. Am. Chem. Soc. 134 (2012) 6826–6833.
[26] S.W. Tao, J. Canales–Vázquez, J.T.S. Irvine, Chem. Mater. 16 (2004) 2309–2316.
[27] W. Zhou, J. Sunarso, J. Motuzas, F.L. Liang, Z.G. Chen, L. Ge, S.M. Liu, A. Julbe, Z.H. Zhu, Chem. Mater. 23 (2011) 1618–1624.
[28] A. Aguadero, D. Pérez–Coll, J.A. Alonso, S.J. Skinner, J. Kilner, Chem. Mater. 24 (2012) 2655–2663.
[29] K.T. Lee, A. Manthiram, Chem. Mater. 18 (2006) 1621–1626.
[30] T. Montini, M. Bevilacqua, E. Fonda, M.F. Casula, S. Lee, C. Tavagnacco, R.J. Gorte, P. Fornasiero, Chem. Mater. 21 (2009) 1768–1774.
[31] A. Manthiram, J. Kim, Y.N. Kim, K. Lee, J. Electroceram. 27 (2011) 93–107.